Sensors and Materials, Vol. 32, No. 9 (2020) 3083–3094
MYU Tokyo

S & M 2324

Flexible-substrate Fluxgate Current Sensor Based on MEMS Technology

Yang Shanglin* and Fan Rong

School of Electrical and Information Engineering, North Minzu University,
Yinchuan, Ningxia 750021, People's Republic of China

(Received December 15, 2019; accepted August 26, 2020)

Keywords: current sensor, fluxgate, MEMS, flexible substrate, soft magnetic material core

A method of preparing a flexible-substrate fluxgate based on MEMS technology was proposed, and the prepared flexible-substrate fluxgate was applied as a current sensor for online measurement. On the basis of MEMS technology, we combined the high precision and high stability of the fluxgate with the flexible and extension characteristics of the substrate to prepare a fluxgate current sensor. This flexible-substrate fluxgate current sensor not only has high precision, but also has the advantage of convenient online measurement of a Rogowski coil.

1. Introduction

The measurement of electric current is widely required in smart grids, new energy systems, electric vehicles, medical equipment, high-speed trains, and electrical instrumentation,[1] where shunt resistance sensors, Hall sensors, anisotropic magnetoresistance sensors, giant magnetoresistance sensors, current transformers, fluxgate sensors, optical fiber sensors, and Rogowski coils are commonly used as measuring sensors, as discussed in two excellent review papers.[1,2] Owing to the large power dissipation and size, shunt resistance is not suitable for large-current measurement, and contactless measurement is attracting increasing attention. Depending on whether the contactless measurement involves a magnetic core, the fluxgate sensors can be divided into current sensors having a core and coreless sensor arrays (or gradiometers). Compared with other contactless current sensors, fluxgate current sensors have superior characteristics in terms of AC–DC measurement, measurement accuracy, sensitivity, and temperature stability.[3–5] To improve the anti-interference ability of fluxgate current sensors, they are usually designed with three structures: a closed-loop core structure, a magnetic gradiometer or sensor array, and a magnetic yoke with a small gap where a magnetic sensor is placed.

The most common form of fluxgate current sensors has a closed-loop core with a measured conductor inside or a closed yoke with sensors. Other current sensors have been fabricated by MEMS or printed circuit board processes, in which the measured conductor is wound on[6] or sandwiched between the core.[7,8] They have poor anti-interference with the external

*Corresponding author: e-mail: ysl029@163.com
https://doi.org/10.18494/SAM.2020.2737

ISSN 0914-4935

magnetic field owing to the small cross-sectional area of the adopted core.[9] The loop core of a high-permeability ferromagnetic material can focus the magnetic field produced by the measured current. Hence, the flux in the test will not depend on the location of the conductor that is tested. This is also the reason why a sensor with a yoke gap has less resistance against interference. Meanwhile, this type of sensor can maintain a high demagnetization factor against an external magnetic field owing to its core with a high cross-sectional area. To broaden the measurement frequency range, a core was added to a fluxgate current sensor on the basis of the transformer principles, and the measurement of high-frequency current can be completed as the fluxgate sensor bandwidth is subject to excitation frequency. In 2010, a sensor of this type with a biaxial fluxgate closed-loop current sensor (named HPCT) was developed by LEM Company.[10,11] To improve the shortcoming of a very large power consumption of this type of device, a low-power switching power supply and a switch amplifier can be used to achieve the excitation and compensation circuits.[12–14] Moreover, other researchers had presented other methods to improve its performance, such as rearranging the core position to improve its shielding against external magnetic field interference[15] and adopting a new excitation method,[16] a new signal extraction method,[17] a novel detection method,[18] or control strategy.[19] Also, there are many practical applications in which a sensor chip is placed in a gap on a closed magnetic conductor for measurement. If a feedback circuit is adopted, the measurement accuracy and stability can be increased. However, compared with a fully closed core loop, sensors with gaps have a stronger temperature dependence.[9]

A gradiometer or an array of current sensors is an alternative for current measurement where space and power limitations preclude the use of a magnetic yoke.[20] Such devices perform magnetic field measurements in accordance with the ampere loop rule. A gradiometer is often used, which has good suppression on a uniform magnetic field but its obvious defect is its low ability to suppress the external current. A gradiometer consisting of two current sensors[21] placed above the U-shaped conductor being tested can provide a good rejection of uniform and non-uniform magnetic field perturbations,[22] although a ring sensor array, such as that with four or eight sensors evenly distributed around the circumference of a test conductor, is another commonly used form. If the sensor outputs are simply averaged, the suppression of the external interference of such sensors is the same as that of gradiometers.[23] The use of more complicated signal processing methods will immensely improve the efficiency of suppressing the external interference of the sensor regardless of the position of the measured current.[24,25] Rectangular and circular fluxgate current sensor arrays are used to measure the current, and it has been shown that the more sensors used, the higher the measurement accuracy.[26,27] However, because the range of measurement is limited by the measured distance, they cannot measure a large current. Therefore, a measurement method involving a sensor chip inside a busbar provides a practical solution in which the distance between two sensors can be adjusted to expand the measurement range and improve the measurement accuracy because of the use of multiple sensors.[28–30]

In addition to the traditional current clamp sensor, which can form an open magnetic circuit, a flexible sensor can form a closed loop because it can be bent into a perfect ring. The most popular flexible current sensor is the Rogowski coil, which enables easy online

measurement and is insensitive to external interference and the surrounding tested conductor but requires accurate winding. A traditional Rogowski coil measures only alternating current and requires an exact integrator at the output. In 2009, Vourc'h *et al.*[31] filled a Rogowski coil with a superparamagnetic powder to form a current sensor and measured AC and DC currents on the basis of the fluxgate principle. Owing to the poor ferromagnetic properties of the superparamagnetic powders, such sensors are only suitable for measuring large currents. We combined the advantage of a fluxgate sensor for high-precision AC and DC measurements and that of a Rogowski coil, which can be bent to form a closed loop, making it robust against external interference. In this paper, a fluxgate current sensor based on a flexible substrate is proposed. It is expected to achieve high-precision online current measurement.

2. Design and Optimization

A fluxgate sensor is a vector sensor for measuring magnetic fields. Its ferromagnetic core is made to work periodically at two poles of magnetic saturation by winding an excitation coil on it. It has the ability to modulate the external magnetic field with the excitation magnetic field to detect the external magnetic field on the basis of the nonlinear magnetic characteristics of the ferromagnetic core. From the relationship between the excitation magnetic field and the direction of the measured magnetic field, fluxgate sensors can be divided into parallel- and orthogonal-excitation fluxgate sensors. To form a nearly closed magnetic loop after bending, in this study, the double-core fluxgate structure shown in Fig. 1 is designed to be composed of four coils wound on an elongated core.

On the basis of previous research results obtained with a voltage-excitation fluxgate model[32] with sensitivity and power consumption as the objective functions, the related parameters of the drive coil, induction coil, core, and excitation condition of the double-core fluxgate shown in Fig. 1 were simulated using SPICE software to validate the theoretical selection of parameters in the designed sensor in the follow-up MEMS process.

To explain the parameter settings in the simulation in this section, some parameter definitions, variable parameters, and constant parameters used in the simulation of the double-core fluxgate (Fig. 2) are given in Tables 1, 2, and 3, respectively. These simulation parameters

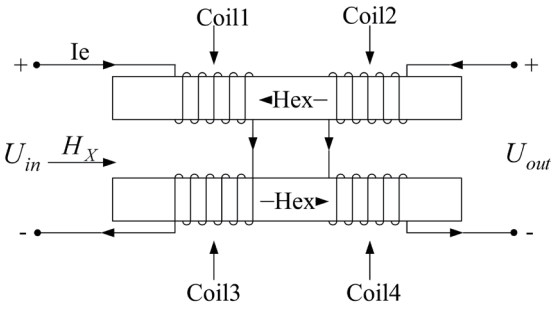

Fig. 1. Double-core fluxgate.

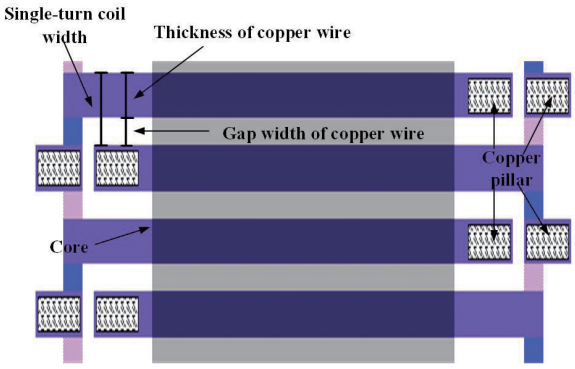

Fig. 2. (Color online) Mask layout of double-core fluxgate (local).

Table 1
Definition of simulation parameters of double-core fluxgate.

Parameter	Symbol	Definition
Width of single-turn coil	d	Sum of copper wire width and gap width in single-turn coil, i.e., d = copper wire width + gap width, as shown in Fig. 2.
Single-turn coil wire duty cycle	k_1	Ratio of copper wire width to single-turn coil width, namely, k_1 = copper wire width/single-turn coil width, as shown in Fig. 2.
Ratio of numbers of primary and secondary coils	k_2	Ratio of number of turns of induction coil to number of turns of excitation coil, namely, k_2 = number of turns of induction coil/number of turns of excitation coil.

Table 2
Parameters of simulation variables of double-core fluxgate.

Parameters of coil						
Parameter	Thickness of copper wire	Single-turn coil width d	Duty ratio of single-turn coil wire k_1	Ratio of numbers of primary and secondary coils k_2		
Initial value	5 μm	100 μm	0.6	1		
Parameters of core						
Parameter	Saturation magnetic induction intensity B_s	Coercive force H_c	Maximum relative permeability μ_r	Length	Width	Thickness
Initial value	1.057 T	70 A/m	15927	30 mm	1 mm	5 μm
Parameters of excitation						
Parameter	Voltage amplitude	Excitation frequency	Waveform	External field		
Initial value	0.5 V	1 kHz	Sine wave	50 A/m		

Table 3
Constant simulation parameters of double-core fluxgate.

Parameter	Symbol	Value	Parameter	Symbol	Value
Copper resistivity	P	1.7×10^{-8} Ω·m	Vacuum permeability	μ_0	$4\pi \times 10^{-7}$ H/m
Vacuum dielectric constant	ε_0	8.85×10^{-12} F/m	Relative permittivity of polyimide	ε_r	4

include independent parameters and derived parameters, including the saturation magnetic induction intensity of the core material; maximum relative permeability; coercive force; core length, width, and thickness; line duty cycle k_1; primary coil ratio k_2; copper wire thickness; single-turn coil width d; and constant parameters. By using the size of the dual-core fluxgate, resistance definition formula, inductance definition formula, capacitor definition formula, and demagnetizing factor formula,[33] one can further calculate the number of turns of the excitation coil, the number of turns of the induction coil, the actual magnetic permeability, resistance, inductance, mutual inductance, and capacitance in the model of the voltage-excitation fluxgate. What needs to be emphasized here is that as the fluxgate is prepared by a MEMS process under existing process conditions, the excitation coil and induction coil of the three-dimensional structure are wound alternately, which makes the magnetization more uniform. The total number of coil turns (the sum of the number of turns of the excitation coil and the number of turns of the induction coil) is the length of the core divided by the width of a single-turn coil. Polyimide is used as the insulation layer between the coils and between the coils and the core. To study the effect of the variable parameters listed in Table 2 on the fluxgate input and output performances, the value of only one variable was changed in each simulation optimization process while the other variables remained unchanged.

In accordance with the above simulation results of the SPICE model based on the voltage excitation fluxgate, the fluxgate sensor is designed to have an elongated ferromagnetic core with alternating winding of the excitation coil and induction coil. The specific structure parameters are shown in Table 4.

3. Design and Fabrication

In this study, the MEMS process is adopted to fabricate a flexible-substrate fluxgate sensor pasted with a cobalt-based amorphous strip core, as shown in Fig. 3. The following is the process flow. Silicon of 500 μm thickness was selected as the substrate and prepared by wet oxidation with 300-nm-thick silicon dioxide as the sacrificial layer for subsequent stripping of polyimide, as shown in Fig. 3(a). The silicon dioxide was coated with a layer of polyimide by a rotary coating process, and the polyimide was treated by imidization. A polyimide film layer of 14 μm thickness was finally obtained as the substrate support layer of the flexible device, as shown in Fig. 3(b). The surface of the polyimide layer was etched by sputtering to generate organic groups on the surface of the polyimide and increase the surface roughness, thereby increasing the adhesion of polyimide to the deposited metal. A layer of titanium metal was prepared on the polyimide by a lift-off process using a bottom copper coil mask. As the adhesion layer, the titanium layer further increases the adhesion between the bottom copper coil and the polyimide layer. Copper film was prepared by magnetron sputtering as the seed layer for electroplating. The bottom copper coil was prepared by an electroplating process. A layer of an AZ4620 photoresist with a thickness of 4 μm was coated on the copper seed layer. A copper coil of nearly 4 μm thickness was then plated in a plating tank [see Fig. 3(c)]. A copper connection pillar was prepared by an electroplating process. An AZ4620 photoresist of 8 μm thickness was further deposited by spin-coating onto the upper layer, and a copper connection pillar mask was used to pattern the photoresist. Then, a copper connection pillar of 8–10 μm thickness was prepared by a copper plating process. The photoresist was removed, and the copper seed layer was removed by wet etching [as shown in Fig. 3(d)]. The polyimide layer was deposited by spin-coating and then subjected to a planarization process [as shown in Fig. 3(e)]. The thinned cobalt-based amorphous strip core was pasted onto the polyimide layer. First, the original cobalt-based amorphous strip was corroded by a wet etching process to reduce its thickness from 25 to about 5 μm. Then, a layer of a 4-μm-thick AZ4620 photoresist was coated onto the silicon chip and baked before processing. The thinning cobalt-based amorphous strip was pasted manually onto the corresponding core position using the viscous photoresist, and the silicon wafer was baked at 90 °C for 15 min to solidify the paste. The polyimide layer was

Table 4
Design parameters of double-core fluxgate sensor.

Parameter	Length of core	Width of core	Thickness of core	Duty ratio of single-turn coil wire k_1	Number ratio of primary to secondary coils k_2	Single-turn coil width d	Thickness of copper wire
Value	30 mm	3 mm	5 μm	0.6	1	300 μm	6 μm

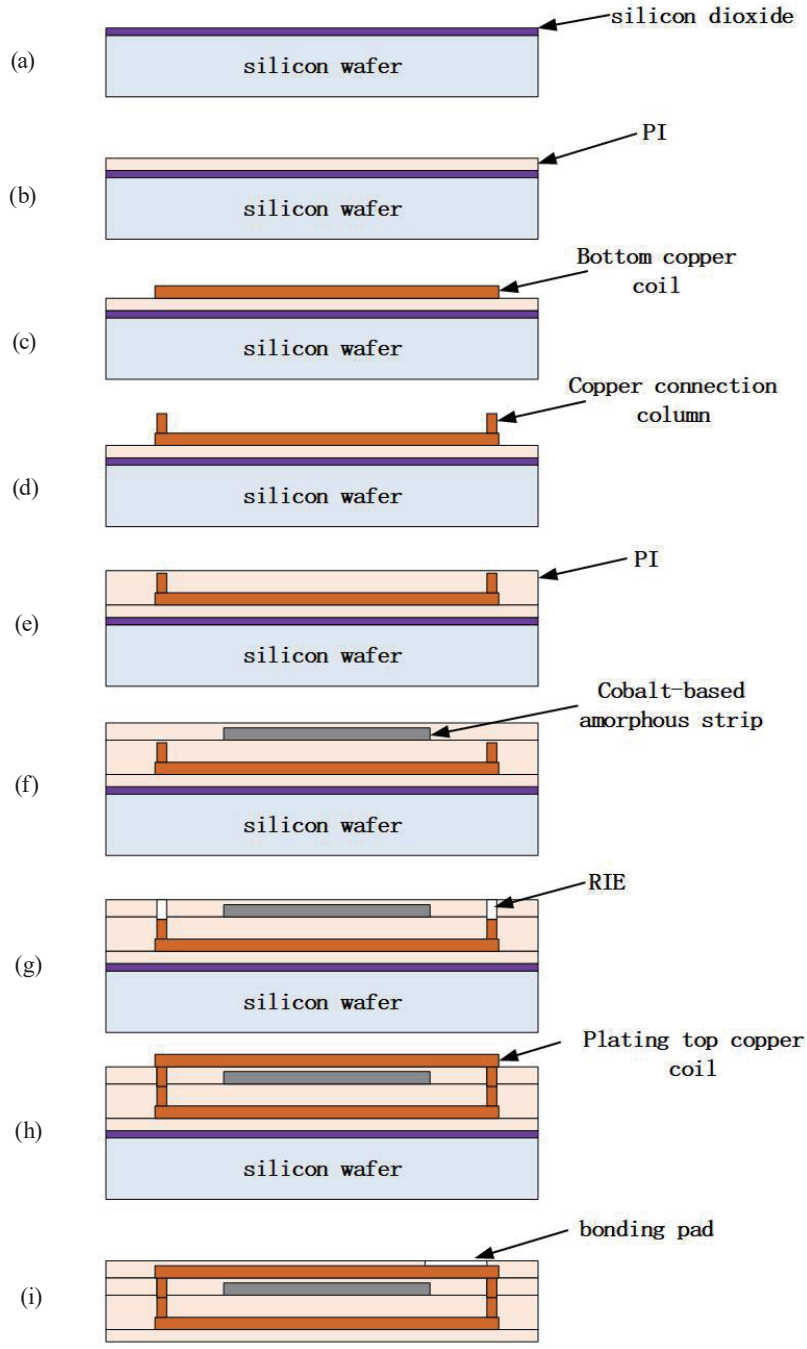

Fig. 3. (Color online) MEMS process for fabricating flexible substrate fluxgate sensor with pasted cobalt-based amorphous strip core.

deposited by spin-coating and subjected to a planarization process. Note here that the final stage of imidization was at 200 °C for 1 h[34] to prevent the cobalt-based amorphous core from causing the deterioration of the soft magnetic properties [see Fig. 3(f)]. The copper mask for reactive-ion etching (RIE) was prepared. Finally, the copper film not covered by a photoresist

was removed by a wet etching process. RIE was carried out to etch the polyimide layer until all the copper connection columns were exposed, then etching was stopped [as shown in Fig. 3(g)]. The upper copper coils were electroplated. Finally, the photoresist was removed, and the copper seed layer was removed by a wet etching process [as shown in Fig. 3(h)]. The polyimide layer was deposited by spin-coating, the pad and groove were etched, and then the polyimide layer was solidified. To prevent the oxidation of the pad, a metal that is not easily oxidized, such as titanium, can be sputtered onto the pad by a lift-off process. The device was split along the groove and stripped. In the stripping stage, the device was immersed in HF solution of 50% concentration, and the bottom polyimide layer was removed from the silicon chip by wet etching the silicon dioxide until the flexible device was completely removed from the silicon chip [as shown in Fig. 3(i)]. The leads were welded on the pad. As the base material was a flexible polyimide material, it was not possible to use a bonding machine to make the lead wire on the pad. Here, a pad was designed to have a large area, and the lead wire was welded onto the pad by normal electric soldering iron welding technology.

The fluxgate of the flexible substrate fabricated by the MEMS process without the substrate removed by stripping is shown in Fig. 4. The positions of the core, coil, and solder pad are marked in Fig. 3. The fluxgate is used as a magnetic field sensor here. The flexible-substrate fluxgate after stripping, which is used as a current sensor, is shown in Fig. 5. The flexible-substrate fluxgate adopts the parallel excitation mode. The primary coil is alternately wound. The line width of the coil is 180 μm, the gap is 120 μm, the total number of turns of the coil is 100, the turn ratio of the primary coil to the secondary coil is 1, the thickness of copper wire is 4 μm, the rod core is 30 mm long and 3 mm wide, the thickness of the core with pasted cobalt-based amorphous strips is about 5 μm, and the size of the welding plate is 1350 × 1350 μm^2. The purpose of setting more bonding pads is to prevent coil impassability and overall device unavailability. After the devices were tested, the resistances of the excitation coil and induction coil were mostly about 10 Ω, and the overall device area was 15 × 34 mm^2.

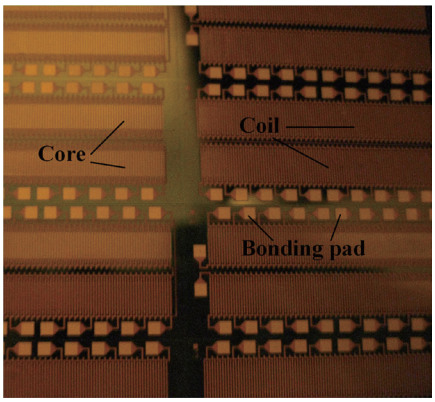

Fig. 4. (Color online) Photograph of unstripped flexible-substrate fluxgate sensor fabricated by MEMS process.

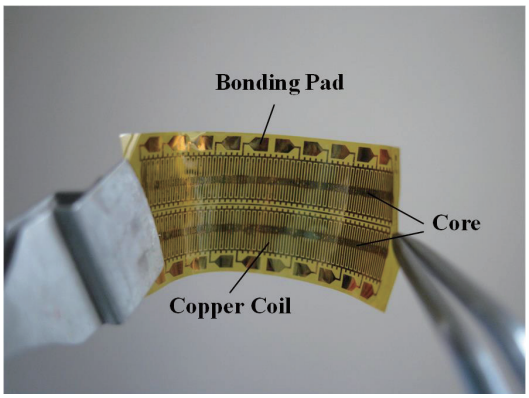

Fig. 5. (Color online) Photograph of flexible-substrate fluxgate sensor fabricated by MEMS process.

4. Test Results

4.1 Test equipment

To measure the samples, a fluxgate sensor performance test system was built. Figure 6 shows the measurement system. The excitation signal is generated by a signal generator (Agilent 33220A) and a power amplifier (NF HSA4011) in series. To measure the effective excitation current, a galvanometer (Agilent 34401A) is connected in series to the excitation circuit. When the fluxgate sensor is used as a current sensor, as shown in Fig. 7, the fluxgate sensor with a flexible substrate is pasted onto a cylindrical support skeleton. The two ends of the core of the sensor with the flexible substrate are close together to close the magnetic circuit, so that the ability to suppress the influence of currents external to the sensor and the influence of the position of the measured conductor on the current can be enhanced. Finally, the measured current is passed through the center of the support skeleton. The measured current is supplied by a DC power supply, and a series galvanometer (Agilent 34401A) is used to calibrate the measured current. This galvanometer is a multipurpose meter with 0.1% accuracy in measuring the DC within a 3 A range. An Agilent Infiniium 54830D oscilloscope or a Tektronix RSA 5103A spectrum analyzer is connected to the induction coil of the fluxgate to analyze the output signal or noise. The whole system is in the open-loop state. The two ends of the induction coil are directly connected to the oscilloscope, and the sensor is neither compensated for nor tuned.

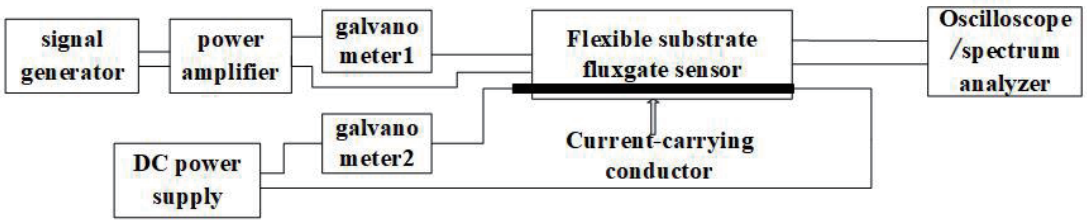

Fig. 6. Measurement system of flexible-substrate fluxgate current sensor.

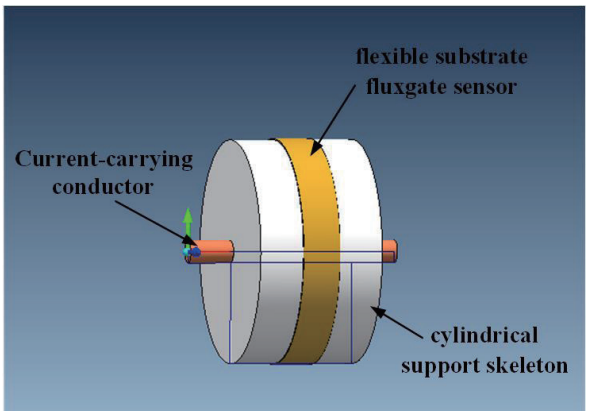

Fig. 7. (Color online) Measurement schematic of flexible-substrate fluxgate current sensor.

4.2 Test results

4.2.1 Effects of excitation current on sensitivity and linear range

Under sinusoidal excitation with a frequency of 500 kHz and an effective excitation current of 100, 200, 300, or 400 mA, the second-harmonic amplitude of the induction coil of the flexible-substrate fluxgate current sensor is measured and the results are shown in Fig. 8 and Table 5. It can be seen that with increasing effective excitation current, the sensitivity of the sensor increases gradually. In contrast, the linear range of the sensor decreases gradually. This trend occurs because the flexible-substrate fluxgate current sensor with a core of cobalt-based amorphous strips more easily reaches the saturation state when the excitation current increases, which leads to the second-harmonic sensitivity gradually increasing to the optimal value. When the excitation current is larger than the optimal value, the second-harmonic sensitivity decreases and the fourth-harmonic sensitivity increases, while the narrow linear range is caused by the increase in core permeability when the cores become saturated in advance.

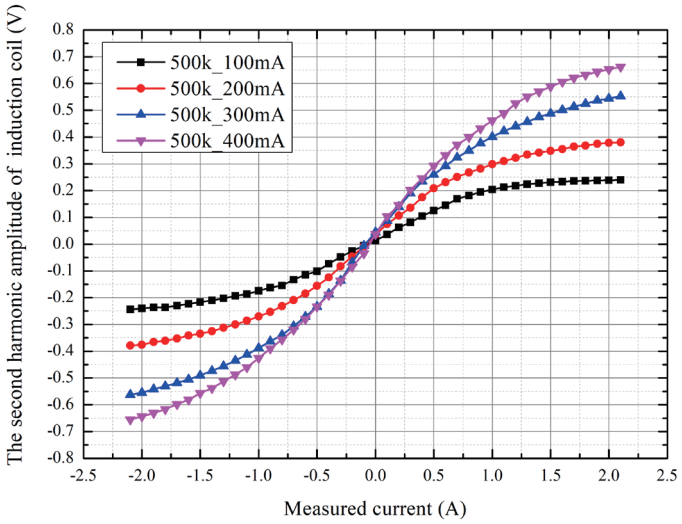

Fig. 8. (Color online) Second-harmonic amplitude as a function of the measured current under different excitation currents.

Table 5

Sensitivity and linear range of sensors with different excitation currents.

Effective excitation current (mA)	Sensitivity (V/A)	Linear range (A)	R^2
100	0.1936	±1.2	0.99119
200	0.3263	±0.9	0.99172
300	0.4644	±0.8	0.99058
400	0.5034	±0.8	0.99563

4.2.2 Effects of different excitation frequencies on sensitivity and linear range

Under sinusoidal excitation with an effective excitation current of 400 mA and a frequency of 100, 200, 500, or 1000 kHz, the second-harmonic amplitude of the induction voltage of the flexible-substrate fluxgate current sensor is measured while varying the measured current; and the results are shown in Fig. 9 and Table 6. It can be seen that as the excitation frequency increases from 100 to 1000 kHz, the sensitivity of the flexible-substrate fluxgate current sensor reaches a maximum at 500 kHz. At the same time, the linear range tends to decrease with increasing excitation frequency. The cause of this phenomenon is the decrease in permeability owing to losses of the amorphous core.

4.2.3 Discussion

When selecting a high-sensitivity fluxgate current sensor, the excitation frequency should be 500 kHz and the effective excitation current should be 400 mA. The power consumption of the flexible-substrate cobalt-based amorphous core fluxgate current sensor is calculated to be 1.6 W. The reason for the high power consumption is that the number of turns per unit length is small and the resistance of the excitation coil is large. After improving the process level, the power consumption is expected to be reduced.

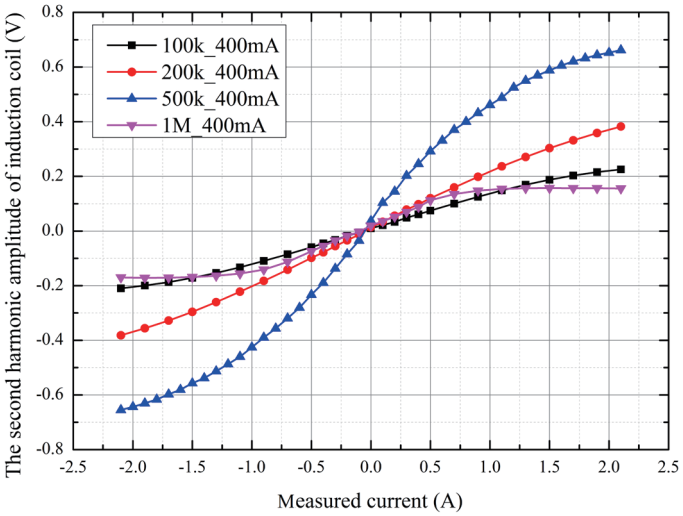

Fig. 9. (Color online) Second-harmonic amplitude as a function of the measured current at different excitation frequencies.

Table 6
Sensitivity and linear range of sensors at different excitation frequencies.

Excitation frequency (kHz)	Sensitivity (V/A)	Linear range (A)	R^2
100	0.1255	±1.5	0.99841
200	0.1947	±2.1	0.99643
500	0.5034	±0.8	0.99058
1000	0.1796	±0.7	0.99785

5. Conclusion

In this paper, a method of preparing a flexible-substrate fluxgate based on MEMS technology was proposed. A fluxgate current sensor with a cobalt-based amorphous strip core and 3D spiral excitation and sensing coils is developed, and it can be bent for online current measurement. When using 500 kHz sinusoidal excitation, the sensitivity reached 0.5034 V/A, and the power consumption of the fluxgate current sensor was 1.6 W. Compared with those described in Ref. 7, in which a planar fluxgate current sensor prepared by a printed circuit board process was reported, the sensitivity of the sensor increased by about 2.5 times and the power consumption decreased by 40%. This new current sensor can be used in, for example, current detection, flexible electronics, biomedical applications, wearable sensors, small-robot control, nondestructive detection, magnetic marker detection, and aircraft navigation. In the future, a fluxgate array can be used to measure current online through the MEMS process, and the performance of the current sensor is expected to be greatly improved by adopting a signal processing process.

Acknowledgments

This work was supported by a key scientific research project of North Minzu University in 2017 on the mechanism and power consumption of a planar coil fluxgate microsensor based on a demagnetizing field view (No. 2017KJ12).

References

1 P. Ripka: Meas. Sci. Technol. **21** (2010) 1. https://doi.org/10.1088/0957-0233/21/11/112001
2 S. Ziegler, R. C. Woodward, H. H. C. Iu, and L. J. Borle: IEEE Sens. J. **9** (2009) 354. https://doi.org/10.1109/jsen.2009.2013914
3 P. Ripka: Magnetic Sensors and Magnetometers (Artech House, Boston·London, 2001) pp. 75–76, 78–80, 85–90, 94–97, 112.
4 P. Ripka and M. Janosek: IEEE Sens. J. **10** (2010) 1108. https://doi.org/10.1109/jsen.2010.2043429
5 S. Tumanski: Handbook of Magnetic Measurements (CRC Press, Boca Raton, 2011) pp. 6–8, 20, 160.
6 Y. Fujiyama, Y. Yamada, H. Kikuchi, M. Yamaguchi, and K. Arai: IEEE Trans. Magn. **33** (1997) 3406. https://doi.org/10.1109/20.617959
7 T. O'Donnell, A. Tipek, A. Connell, P. McCloskey, and S. C. O'Mathuna: Sens. Actuators, A **129** (2006) 20. https://doi.org/10.1016/j.sna.2005.09.044
8 A. Tipek, T. O'Donnell, A. Connell, P. McCloskey, and S. C. O'Mathuna: Sens. Actuators, A **132** (2006) 21. https://doi.org/10.1016/j.sna.2006.06.057
9 P. Ripka: Tm-Technisches Messen **86** (2019) 586. https://doi.org/10.1515/teme-2019-0032
10 Isolated Current and Voltage Transducers: Characteristics–Applications–Calculations: http://www.lem.com/images/stories/files/Products/P1_5_1_industry/CH24101E.pdf (accessed May 2004).
11 C. Gudel: The World of Power Supply (2010) 38. https://doi.org/CNKI:SUN:DYSE.0.2010-08-039
12 M. Roman, G. Velasco, A. Conesa, and F. Jerez: 2008 IEEE Power Electronics Specialists Conf. (2008) 535. https://doi.org/10.1109/pesc.2008.4591984
13 G. Velasco-Quesada, M. Roman-Lumbreras, A. Conesa-Roca, and F. Jerez: IEEE Sens. J. **11** (2011) 280. https://doi.org/10.1109/jsen.2010.2054831
14 S. Veinovic, M. Ponjavic, S. Milic, and R. Djuric: IET Circuits Devices Syst. **12** (2018) 215. https://doi.org/10.1049/iet-cds.2017.0324
15 X. G. Yang, B. Zhang, Y. H. Wang, Z. G. Zhao, and W. L. Yan: J. Appl. Phys. **111** (2012). https://doi.org/10.1063/1.3677200

16 W. Teppan and D. Jobling: 2018 Conf. Precision Electromagnetic Measurements (2018). https://doi.org/10.1109/CPEM.2018.8501163
17 W. Yao: Reaseach on Detecting Technology of Residual Currents under Complicated Waveform Conditions (Publisher, Tianjin, 2012) p. 43. https://doi.org/10.7666/d.D464716
18 N. Wang, Z. H. Zhang, Z. K. Li, Q. He, F. P. Lin, and Y. F. Lu: IEEE Sens. J. **16** (2016) 2971. https://doi.org/10.1109/jsen.2016.2524042
19 X. L. Tian, Q. Y. Qian, and W. Fu: 2018 Int. Conf. Power System Technology (2018) 1056. https://doi.org/10.1109/POWERCON.2018.8601521
20 P. Ripka: J. Optoelectron. Adv. Mater. (2004) 587.
21 W. H. Campbell and J. E. Zimmerman: IEEE Trans. Geosci. Remote Sens. **18** (1980) 244. https://doi.org/10.1109/tgrs.1980.4307498
22 A. Msaed, M. Tawk, Y. Zaatar, and D. Zaouk: Design of an Accuracy Current Sensor Using Amorphous Fine Wire of FeCoSiB: In Advances in Innovative Materials and Applications (Trans Tech Publications Ltd, Stafa-Zurich, 2011) p. 423. http://doi.org/10.4028/www.scientific.net/AMR.324.423
23 P. Ripka, P. Kaspar, and J. Saneistr: Przem. Elektrotechniczny **88** (2012) 38.
24 R. Bazzocchi and L. Di Rienzo: Sens. Actuators, A. **85** (2000) 38. https://doi.org/10.1016/S0924-4247(00)00321-6
25 L. Di Rienzo, R. Bazzocchi, and A. Manara: IEEE Trans. Instrum. Meas. **50** (2001) 1093. https://doi.org/10.1109/19.963165
26 A. Chirtsov, P. Ripka, and J. Vyhnanek: 2018 IEEE Sens. (2018) 1. https://doi.org/10.1109/ICSENS.2018.8589563
27 V. Grim, P. Ripka, and J. Fischer: 2019 IEEE Sensors Applications Symp. (2019). http://doi.org/10.1109/SAS.2019.8706029
28 P. Ripka, M. Pribil, V. Petrucha, V. Grim, and K. Draxler: IEEE Trans. Magn. **52** (2016). https://doi.org/10.1109/tmag.2016.2540523
29 P. Ripka, V. Grim, and V. Petrucha: IEEE Trans. Magn. **53** (2017). https://doi.org/10.1109/tmag.2016.2620959
30 P. Ripka and A. Chirtsov: IEEE Trans. Magn. **54** (2018). https://doi.org/10.1109/tmag.2018.2844254
31 E. Vourc'h, P.-Y. Joubert, and L. Cima: Progress In Electromagnetics Research **99** (2009) 323. https://doi.org/10.2528/PIER09102006
32 S. L. Yang, S. B. Liu, W. G. Feng, B. Guo, X. W. Hou, and J. P. Li: IET Sci. Meas. Technol. **7** (2013) 145. https://doi.org/10.1049/iet-smt.2013.0005
33 X. Zhang and Y. Lu: Fluxgate Technology (National Defense Industry Press, Beijing, 1995) p. 2.
34 B. Guo, S. B. Liu, S. L. Yang, X. W. Hou, and J. P. Li: J. Funct. Mater. **44** (2013) 2719. https://doi.org/10.3969/j.issn.1001-9731.2013.18.030

About the Authors

Yang Shanglin received his B.S. degree from Northwest A&F University, China, in 2007, and his M.S. and Ph.D. degrees from Northwestern Polytechnical University, China, in 2009 and 2016, respectively. Since 2016, he has been a lecturer at North Minzu University, China. His research interests are in MEMS and magnetic sensors. (ysl029@163.com)

Fan Rong received her B.S. and M.S. degrees from Taiyuan University of Technology, China, in 2001 and 2006, respectively. From 2006 to 2015, she was a lecturer at North Minzu University, China. Since 2015, she has been an associate professor at this university. Her research interests are in signal and information processing. (fanrong11@126.com)